J. Am. Soc. Mass Spectrom. (2011) 22:1260–1272
DOI: 10.1007/s13361-011-0133-9

RESEARCH ARTICLE

# Gas Phase Reactions of 1,3,5-Triazine: Proton Transfer, Hydride Transfer, and Anionic σ-Adduct Formation

John M. Garver,[1] Zhibo Yang,[1] Shuji Kato,[1] Scott W. Wren,[1,2] Kristen M. Vogelhuber,[1,2] W. Carl Lineberger,[1,2] Veronica M. Bierbaum[1,2]

[1]Department of Chemistry and Biochemistry, University of Colorado, Boulder, CO 80309, USA
[2]JILA, University of Colorado and the National Institute of Standards and Technology, Boulder, CO 80309, USA

**Abstract**

The gas phase reactivity of 1,3,5-triazine with several oxyanions and carbanions, as well as amide, was evaluated using a flowing afterglow-selected ion flow tube mass spectrometer. Isotopic labeling, H/D exchange, and collision induced dissociation experiments were conducted to facilitate the interpretation of structures and fragmentation processes. A multi-step (→ HCN + $HC_2N_2^-$ → $CN^-$ + 2 HCN) and/or single-step (→ $CN^-$ + 2 HCN) ring-opening collision-induced fragmentation process appears to exist for 1,3,5-triazinide. In addition to proton and hydride transfer reactions, the data indicate a competitive nucleophilic aromatic addition pathway ($S_NAr$) over a wide range of relative gas phase acidities to form strong anionic σ-adducts (Meisenheimer complexes). The significant hydride acceptor properties and stability of the anionic σ-adducts are rationalized by extremely electrophilic carbon centers and symmetric charge delocalization at the electron-withdrawing nitrogen positions. The types of anion-arene binding motifs and their influence on reaction pathways are discussed.

**Key words:** Gas phase reactions, 1,3,5-triazine, Hydride transfer, Proton transfer, Meisenheimer complex

## Introduction

The chemical compound 1,3,5-triazine, ($C_3N_3H_3$), also known as s-triazine, is a symmetric six-membered N-heterocyclic aromatic ring consisting of alternating carbon and nitrogen atoms. N-heterocycles are important constituents of many natural and synthetic products (plastics, drugs, petrochemicals, food, paints, etc.) and offer the high-energy-high-density properties desired in energetic materials (explosives, pyrotechnics, propellants, and fuels) [1]. Furthermore, nitrogen ring compounds are biologically relevant as model nucleobases due to their H-acceptor abilities [2] and their role in bioactivity [3]. Triazine derivatives are commonly used in herbicides [4], pharmaceutical products [5, 6] and as light stabilizers in polymers [7, 8]. Many of the unique chemical and physical properties of the triazine compounds arise from the interaction of the carbon atoms with the electron-withdrawing nitrogen atoms within the aromatic ring [2, 9]. While the structure-reactivity relationships of nitroaromatics have been extensively studied, more recently the electrostatic interaction of anions with electron-deficient arenes and heteroarenes has gained interest [10, 11]. Our investigation of the gas phase reactivity of the electrophilic 1,3,5-triazine and the complexes formed during these reactions has revealed significant hydride acceptor properties and proven insightful into anion-arene interactions.

**Electronic supplementary material** The online version of this article (doi:10.1007/s13361-011-0133-9) contains supplementary material, which is available to authorized users.

*Correspondence to:* Veronica M. Bierbaum; *e-mail:* veronica.bierbaum@colorado.edu

Received: 7 February 2011
Revised: 17 March 2011
Accepted: 17 March 2011
Published online: 19 April 2011

Polycyclic or heterocyclic conjugated systems tend to exhibit thermodynamic and kinetic stability [12]. This "aromatic" stability can influence physicochemical properties, as well as the forces that govern reaction pathways [13]. While the incorporation of nitrogen within an aromatic ring has little effect on aromaticity, there are significant effects on reactivity [14]. Typically the л-electron density of an aromatic ring makes it susceptible to reactions by electrophilic agents, however the addition of an electron-withdrawing group activates the compound to nucleophilic attack via a $S_NAr$ mechanism [15]. The $S_NAr$ mechanism is believed to be a two-step addition-elimination pathway which proceeds through a Meisenheimer complex (anionic σ-adduct) intermediate. In solution, these complexes typically serve as reaction intermediates, however, in the gas phase these species can be isolated and characterized in the absence of complicating solvent interactions [16, 17].

Transition states [18] and stable intermediates [19] of anionic σ-adducts have been reported in gas phase reactions. To understand the reactivity of the prototypical $S_NAr$ reaction, Fernández et al. [20] conducted a theoretical investigation of the stability of these structures relative to intrinsic nucleophilicity. Interestingly, unlike aliphatic nucleophilic substitution reactions ($S_N2$), the identity $S_NAr$ reactions (where nucleophile and leaving group are the same) for aromatics with nucleophiles belonging to the same period of the periodic table have almost identical barrier heights. However, in non-identity reactions the exothermicity of reaction provides a thermodynamic driving force which influences barrier heights. The intrinsic stability of the complex is dominated by the nature of the aromatic substrate. During the formation of the anionic σ-adduct, a critical balance between the stabilization due to bond formation and destabilization from the destruction of aromaticity dictates the relative potential energy (minimum or transition state) of the complex. Less stable structures gain stability through more planar orientations through distortions of the typical tetrahedral ($sp^3$) Meisenheimer-type geometry. These findings correlate nicely with the anion-arene interactions described by Hay and Bryantsev [21] and the experimental results of Hiraoka et al. [22].

To ensure common nomenclature in discussions of anion–arene interactions, Hay and Bryantsev have proposed characterization of complexes by geometric features and the degree of covalency [21]. Figure 1 depicts the primary binding motif categories as (a) aryl H-bonding (when acidic hydrogens are present), (b) noncovalent anion–π complexes, (c) weakly covalent σ-adducts, and (d) strongly covalent σ-adducts. "Strongly covalent σ-adducts" have extensive mixing of the anion and arene-type molecular orbitals (MOs) to form the typical tetrahedral ($sp^3$) Meisenheimer-type structures. "Noncovalent anion–л complexes" exhibit ring-centered geometries which are bound with electrostatic forces. Moderate interaction between the anion and arene MOs yields "weakly covalent σ-adducts" with off-center

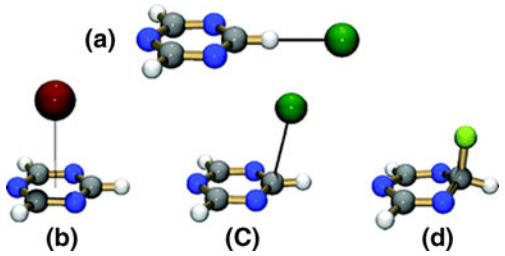


**Figure 1.** Binding modes for complexes of anions with charge-neutral arenes (**a**) C–H hydrogen bonding, (**b**) non-covalent anion–π interaction, (**c**) weakly covalent σ interaction, and (**d**) strongly covalent σ interaction. [21] - Reproduced by permission of The Royal Chemical Society

configurations. Employing these definitions, true electrostatic binding of anions with aryl rings is rare and most supramolecular bonding and solid state interactions display off-center arrangements [10].

Computations suggest that strong nucleophiles produce strongly covalent σ-adducts, while less nucleophilic anions form weakly covalent σ-adducts depending on electron deficiency in the aromatic ring [21]. Gas phase spectroscopic evidence of these two types of structural motifs supports this relationship [23]. The amount of interaction between the electrons of the anion and the л-system is enhanced and stabilized by electron deficiencies in the aromatic ring. The degree of electron deficiency in aryl compounds can be modulated through substitution of electron withdrawing groups, such as –F, –CN, and $–NO_2$. However, electron-withdrawing groups can inductively weaken the strength of hydrogen bonds which enhances the proton transfer processes. Therefore when aryl C–H groups are present, both hydrogen bound anion complexes and anionic σ-adducts must be considered. Studies of substituted benzenes suggest that gas phase nucleophilic attack on the ring is feasible only when the acidity of the aromatic compounds is lower than or comparable to that of the nucleophile [24, 25]. While hydrogen bound complexes may be present at a wide range of relative acidities, the proton transfer channel does not become active until about the same relative acidity range as that of nucleophilic substitution. For highly basic nucleophiles, the proton transfer reaction is significantly favored over the substitution reaction [24, 26].

Depending on the nature of the anion and arene, gas phase reactions have shown the aromatic nucleophilic substitution channel to be in competition with multiple pathways (proton transfer, E2 elimination, $S_N2$, etc.) [26–29]. Of particular interest to our current work is the presence of a hydride transfer channel with 1,3,5-triazine to form a hydride-Meisenheimer complex. Recently, these complexes have been identified in the biodegradation of nitroaromatics [30–34]. Although fragmentation patterns of the hydride-Meisenheimer complex of trinitrotoluene, $[TNT + H]^-$, were studied by Yinon et al., reduction and hydrolysis in their heated source prevented identification of stable hydride

σ-adducts [35]. Other hydride transfer mechanisms for the anionic reductions of carbonyls and activated olefins have been observed in the gas phase [36–40], however to our knowledge hydride transfer to neutral aromatics and stable anionic hydride σ-adducts have not been reported in the gas phase. A computational study by Gronert and Keeffe on factors influencing hydride transfer indicates that electron withdrawing groups increase hydride ion affinity and reaction rates, while resonance lowers barriers to hydride transfer [41]. From this perspective, electrophilic aromatic rings offer intriguing hydride donor and acceptor properties.

In the present study, we investigate the reactivity of 1,3,5-triazine with amide and several oxyanions and carbanions, as well as evaluate the reaction products using collision-induced dissociation. A flowing afterglow-selected ion flow tube (FA-SIFT) mass spectrometer was utilized to measure kinetic data and analyze the dissociation process. Isotopic labeling and H/D exchange experiments were conducted to facilitate the interpretation of fragmentation processes and the structure of products. In addition, theoretical calculations were carried out to elucidate the structure of the intermediates/transition states/products and the driving energetics behind the mechanistic processes. Our results are discussed in terms of relative gas phase acidities, anion-arene interactions, and σ-adduct stability.

## Experimental

### *Ion–Molecule Reactions*

All reactions were carried out using a flowing afterglow-selected ion flow tube (FA-SIFT) mass spectrometer, which has been previously described [42]. Briefly, this instrument consists of four sections: an ion source, an ion selection region, a reaction flow tube, and a detection system. A flowing afterglow ion source is used to produce ions, which are mass selected using the ion selection region quadrupole mass filter prior to injection into the reaction flow tube. Primary anions were prepared by electron ionization (70 eV) of methane and nitrous oxide (2:1 ratio) to produce hydroxide or of ammonia to produce amide. Other ionic reagents were generated by proton abstraction of neutrals by either $NH_2^-$ or $HO^-$. Injected ions are entrained in a flow of helium (200 std $cm^3$ $s^{-1}$, 0.5 Torr) and thermalized to 298 K prior to reactions with neutral reagents that are added through multiple inlets along the length of the reaction flow tube. Ionic reactants and products are analyzed in the detection region using a triple-quadrupole mass filter and an electron multiplier. The reactions are carried out under pseudo-first order conditions (reactant ion ~$10^5$ ions $cm^{-3}$; neutral reactant ~$10^{11}$ molecules $cm^{-3}$), and the reported branching ratios and reaction rate coefficients are the averages of at least three individual measurements. Product branching ratios are determined by extrapolating the observed product yields to zero reaction distance in order to extract the intrinsic ratios due to primary reactions. The reported reaction efficiencies are the experimental rate constant divided by the calculated collision rate constant ($Eff=k_{expt}/k_{col}$). Collision rate constants were calculated from parameterized trajectory collision rate theory [43]. Error bars represent one standard deviation in the data; absolute uncertainties in these rate constant measurements are ±20%. The detector was tuned to minimize mass discrimination, and no further corrections were made in the analysis.

### *Collision-Induced Dissociation*

The source and selection region of the FA-SIFT mass spectrometer has been previously employed in collision-induced dissociation experiments to investigate fragmentation pathways and estimate dissociation energies [44–46]. Collisional activation is accomplished by injecting the anion or adduct at varied injection energies ($E_{lab}$) of 10–80 eV, defined as the voltage difference between the source flow tube and the injection orifice. Collisions with helium take place in the vicinity of the injection orifice (i.e., SIFT-CID) that connects the quadrupole region and the second flow tube. Nominal center-of-mass collision energies ($E_{cm}$) can be calculated using the relation $E_{cm} = E_{lab} \cdot m_{He}/(m_{He} + m_{ion})$, where $m_{He}$ and $m_{ion}$ are the masses of He and the reactant ion, respectively. However, SIFT–CID occurs under multiple-collision conditions thereby enabling fragmentation at collision energies that are lower than threshold energies. The $E_{cm}$ should thus be taken as the lower bound for the actual internal excitation of the anions. The mass spectra of the precursor and fragment ions were analyzed to elucidate the chemical structures of molecules.

### *H/D Exchange*

Hydrogen/deuterium (H/D) exchange reactions of gas phase ions have proven to be powerful tools for probing ion structures in the FA-SIFT [47, 48]. In our H/D exchange analysis, gaseous $D_2O$ was added near the middle of our reaction flow tube downstream of the first four neutral reactant inlets. The extent of H/D exchange for reactant and product ions was evaluated by *m/z* shifts in the mass spectra.

## Materials

All compounds were obtained from commercial vendors and liquid samples were purified by several freeze-pump-thaw cycles before use. These compounds include 1,3,5-triazine, $C_3N_3H_3$, Aldrich, Milwaukee (Winconsin), USA, 97%; ammonia, $NH_3$, Airgas, Denver (Colorado), USA, 99.9995%; 2-methylpropene, $CH_2=C(CH_3)_2$, Phillips 66, Pasadena (Texas), USA, 99+%; 1,4-diazine, $C_4H_4N_2$, Aldrich, 99+%; furan, $C_4H_4O$, Aldrich, 99+%; pyridine, $C_5H_5N$, Fluka, Milwaukee (Wisconsin), USA, 99.8%; difluoromethane, $F_2CH_2$, Aldrich, 99.7%; fluorobenzene, $C_6H_5F$, Aldrich, 99%; difluorobenzene, $C_6H_4F_2$, Aldrich, 99%; 2-methylfuran, $(CH_3)C_4H_3O$, Aldrich, 99%; 1,4-dimethylbenzene, $(CH_3)_2C_6H_4$, EM Science, Gibbstown (New Jersey), USA, 98%;

cyclopentanol, $C_5H_9OH$, Aldrich, 99%: ethanol, $C_2H_5OH$, Decon Laboratories, King of Prussia, (Pennsylvania), USA, 200 proof; methanol, $CH_3OH$, Aldrich, 99.9%; methanol-$d_4$, $CD_3OD$, CDN Isotopes, Pointe-Claire (Quebec), Canada, 99.8% D; water, $H_2O$, distilled; water, $H_2{}^{18}O$, Cambridge Isotope Laboratories, Andover (Maryland), USA, 80% $^{18}O$; $D_2O$, Cambridge Isotope Laboratories, 99.9% D. The reagents were protected from light and stored under vacuum. Helium buffer gas (99.995%) was purified by passage through a molecular sieve trap immersed in liquid nitrogen.

### *Computational Methods*

Ab initio molecular orbital calculations were carried out with the B3LYP method using the 6-311++G(d,p) and aug-CC-pVTZ basis sets using the Gaussian 03 suite of programs [49]. Frequency calculations were carried out for all species to establish their nature as local minima or transition states. Enthalpy changes were calculated from the energies of the optimized structures, and thermal corrections included for 298 K without any scaling of the calculated vibrational frequencies.

## Results and Discussion

The bimolecular ion-neutral reactions between deprotonated 1,3,5-triazine and oxygen-centered reactants (water, methanol, cyclopentanol, and ethanol), carbon-centered reactants (2-methylpropene, 1,4-dimethylbenzene, 1,4-diazine, pyridine, fluorobenzene, difluorobenzene, furan, and 2-methylfuran), and a nitrogen-centered reactant (ammonia) were investigated with FA-SIFT mass spectrometry. The corresponding reverse processes were also studied, i.e., the reactions of deprotonated oxygen-, carbon-, and nitrogen centered reactants with neutral 1,3,5-triazine. Proton and hydride transfer reactions were observed, however the formation of a collision stabilized adduct/cluster dominated most of the reactions studied. Of significant interest was the type of anion-arene binding motif present within these complexes and the influence of this interaction on reaction pathways.

### *Elucidation of Structure, Mechanisms, and Energetics*

Collision-induced dissociation (CID) mass spectrometry was employed to investigate the key structural features, energetics, and thermochemical properties of our gas-phase ion–molecule reactions. In CID, selected precursor ions are activated by multiple collisions with a buffer gas which increases the internal vibrational and rotational energy of the ion until dissociation occurs. Mass shifts corresponding to isotopic labeling and fragmentation patterns allow the elucidation of structure and insight into reaction and dissociation mechanisms. In a simple bond-breaking process, the dissociation product intensities yield information regarding bond energies within the precursor ion. Coarse decomposition threshold energies can be extracted from energy-dependent precursor ion breakdown curves. However in more complex processes, the product intensities will be associated with activation energies that reflect bond breaking and bond formation. Application of the extended kinetic method to the fragmentation ratios of proton-bound ion complexes allows the relative proton affinity of an unknown to be determined relative to a series of reference bases.

Figure 2a displays the FA-SIFT mass spectrum for the reaction of $HO^-$ + 1,3,5-triazine. The major product ion of the reaction is deprotonated 1,3,5-triazine (*m/z* 80); a small contribution from the stabilized ion-dipole complex is observed at *m/z* 98 ($[HO{\bullet}C_3H_3N_3]^-$). Minor ion peaks at *m/z* 26 ($CN^-$), *m/z* 44, and *m/z* 71 suggest either appreciable contributions from impurities or a fragmentation pathway. Similar ion peaks from CID of the hydroxide-1,3,5-triazine cluster, $[HO{\bullet}C_3H_3N_3]^-$ (Figure 2b) are observed. This suggests that the $HO^-$ + 1,3,5-triazine product ion peaks at *m/z* 26, 44, and 71 originate from the reactant ion-dipole cluster, $[HO{\bullet}C_3H_3N_3]^-$, as opposed to impurities. Further supporting this interpretation is the observed isotopic shift (inset, Figure 2a) of *m/z* 44 to 46 and *m/z* 71 to 73 when $H^{18}O^-$ was utilized in both the reaction and cluster generation. Clearly $^{18}O$ is incorporated into the products and fragments; however this result can be explained through either an electrostatic clustering interaction (*m/z* 44, $[CN^-{\bullet}{\bullet}{\bullet}H_2O]$ and *m/z* 71, $[C_2HN_2^-{\bullet}{\bullet}{\bullet}H_2O]$) or a covalent bonding interaction (*m/z* 44, $[NH{=}CHO^-]$ and *m/z* 71, $[C_2N_2H_3O^-]$).

To resolve the nature of these peaks, the *m/z* 44 ion was generated in the source from the reaction of $HO^-$ + 1,3,5-triazine; unfortunately, the *m/z* 71 ion could not be generated in sufficient quantities to study. Mass selection and injection of the *m/z* 44 ion over an $E_{cm}$ injection energy range of 1–2 eV, resulted only in an ion peak at *m/z* 42. If the *m/z* 44 ion were a water cluster, a peak at *m/z* 26 should have been observed. The peak at *m/z* 42 ($NCO^-$) is consistent with loss of $H_2$ from $NH{=}CHO^-$. CID of the *m/z* 96 ion produced the same *m/z* 42 peak, implying that this ion has a keto-type structure generated from the loss of $H_2$ from an *m/z* 98 covalently bound adduct. Therefore, the peaks at *m/z* 26 ($CN^-$), *m/z* 44 ($NH{=}CHO^-$), and *m/z* 71 ($C_2N_2H_3O^-$) indicate an addition mechanism prior to a ring-opening fragmentation process, signifying the presence of a covalent σ-adduct motif within the stabilized ion-dipole complex.

Figure 2c displays the mass spectrum of the reaction of $CH_3O^-$ + 1,3,5-triazine. The major product ion of the reaction is the hydride transfer product of 1,3,5-triazine to produce a hydride-Meisenheimer complex, $C_3H_4N_3^-$ (*m/z* 82). This product was confirmed by an isotopic shift (inset, Figure 2c) of *m/z* 82 to 83 for the reaction of $CD_3O^-$ with 1,3,5-triazine. Additional peaks show the presence of deprotonated 1,3,5-triazine at *m/z* 80, a stabilized species at *m/z* 112 and minor peaks at *m/z* 26 and 44. CID of the stable species (Figure 2d) does not reveal additional fragmentation pathways.

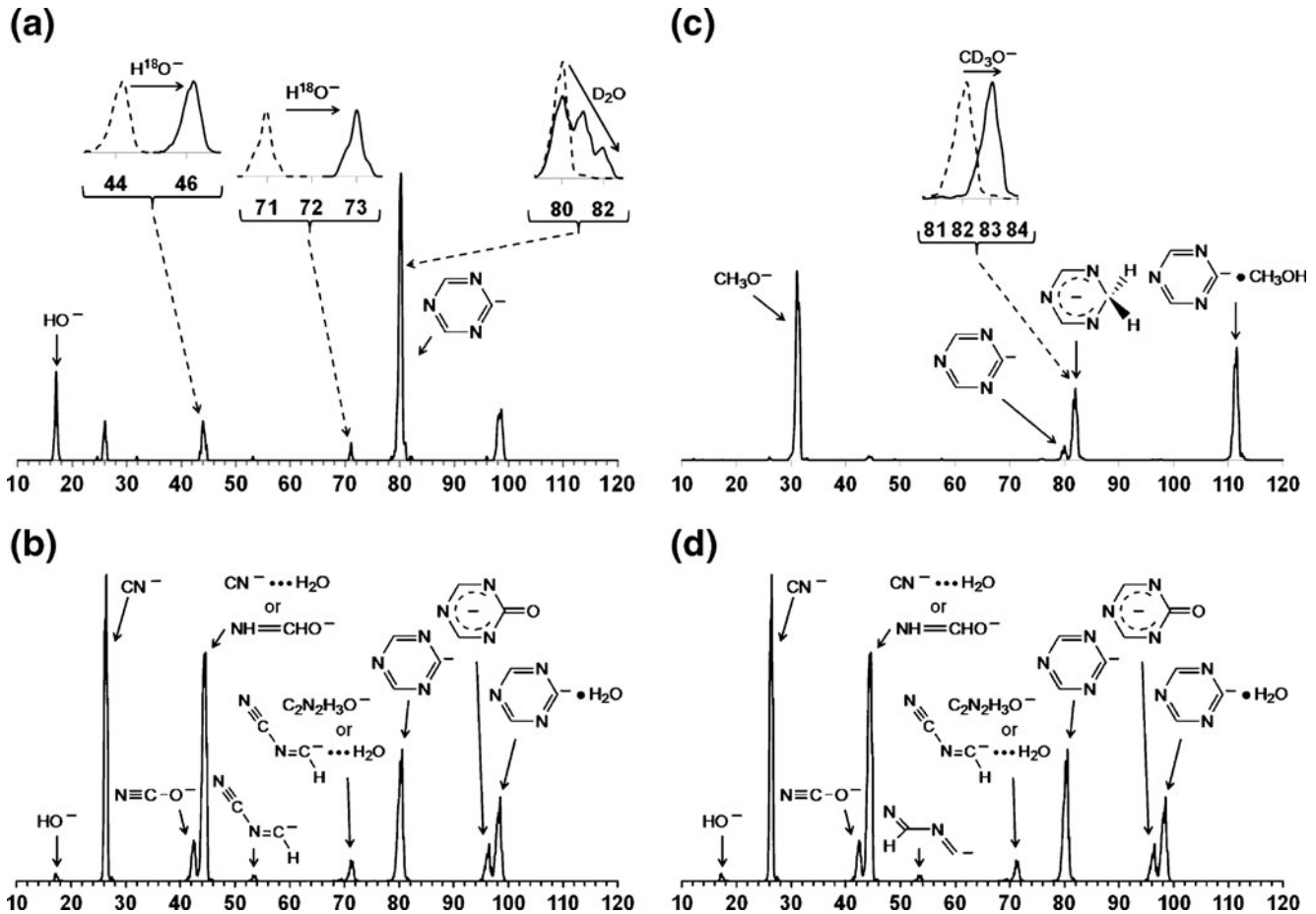


**Figure 2.** FA-SIFT Mass Spectra of (**a**) the reaction of $HO^-$ + 1,3,5-triazine with insets of isotopic shift studies, (**b**) CID of the hydroxide-1,3,5-triazine species, $[HO{\bullet}C_3H_3N_3]^-$, at an $E_{cm}$ injection voltage of 1.2 eV. (**c**) the reaction of $CH_3O^-$ + 1,3,5-triazine with insets of isotopic shift studies, and (**d**) CID of the methoxide-1,3,5-triazine species, $[CH_3O{\bullet}C_3H_3N_3]^-$, at $E_{cm}$ of 0.65 eV

The presence of a ring-opening fragmentation pathway led to concerns that the $C_3H_2N_3^-$ (*m/z* 80) species (Scheme 1) could be the intact 1,3,5-triazinide (1) and/or its ring-opened structure (2). Hydrogen migration during ring opening may give rise to a second ring-opened species (2′).

Producing 1,3,5-triazinide, $C_3H_2N_3^-$, in the source through the reactions of $CH_3O^-$ and $HO^-$ with 1,3,5-triazine allowed the structure of the *m/z* 80 product to be probed by CID and H/D exchange. The injection of 1,3,5-triazinide yielded about 10% $CN^-$ ions even at the lowest injection energy ($E_{cm}$ ~0.5 eV). Figure 3 shows the relative yields of the product ions in CID of the 1,3,5-triazinide anion as a function of SIFT injection energy. As the injection energy increases, more $CN^-$ ions are observed together with a minor amount of *m/z* 53 ions. A nominal CID threshold energy has been estimated from the decomposition behavior of 1,3,5-triazinide to be roughly 1.5 eV (35 kcal $mol^{-1}$) following the calibration procedure described earlier for SIFT-CID involving multiple

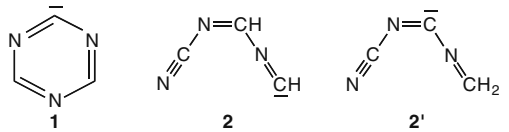


Scheme **1.** Intact and ring-opened $C_3H_2N_3^-$ (*m/z* 80) species

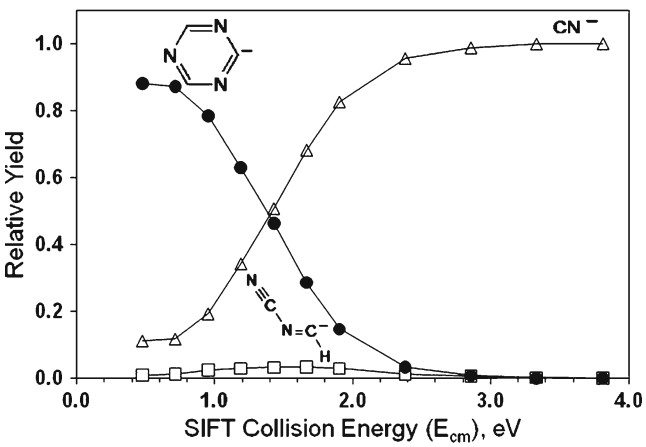


**Figure 3.** Relative yield of the product ions from the SIFT collision-induced dissociation of 1,3,5-triazinide, $C_3H_2N_3^-$, as a function of translational energy in the center-of-mass frame

collisions [50]. The derived value compares qualitatively well with our calculated rate-determining barrier (44.3 kcal $mol^{-1}$) and the experimental dissociation energy for 1,3,5-triazine (40 kcal $mol^{-1}$) [51].

The photodissociation of neutral 1,3,5-triazine to produce three HCN molecules has been attributed to two reaction channels, a simultaneous three-body dissociation mechanism and a consecutive two-body process from a ring-opened structure, which proceeds by the initial formation of HCN and $H_2C_2N_2$ [52]. A similar dissociation scheme (Scheme 2) can be used to describe the fragmentation of 1,3,5-triazinide. The reagent anion proceeds through a ring-opening transition state **TS1**. The ring-opened anion **2** can further fragment via **TS2** to an ion-neutral adduct **3**. After loss of HCN the NC-N=CH$^-$ anion **4** (*m/z* 53) transforms via **TS3** to an ion-neutral adduct **5**, which loses HCN to yield the terminal product ion $CN^-$.

An energy diagram for the decomposition of 1,3,5-triazinide is shown in Figure 4. The ring-opened transition state TS1 has a relatively low bond energy of 29.9 kcal $mol^{-1}$. The diagram assumes that the HCN molecules have been sequentially lost. Interestingly, the observed yield of the NC-N=CH$^-$ anion is minor and the decomposition of 1,3,5-triazinide proceeds primarily to form the terminal anion $CN^-$ even at the lowest collision energy studied. Anions 1, 2, and 2′ have the same mass; however, these structures can be differentiated, in principle, by changes in reaction rate constants and by deuterium exchange reactions. Based on these studies [53], the yield of the ring-opened anion 2 and 2′ is negligibly small following injection of 1,3,5-triazinide; it is possible that collisions with helium sequentially destroy the intermediate species. Alternatively and more probably, the energized species can fragment by a multi-step and/or single-step process in which the species are stabilized by the complexation energy of the fragment ion and neutral product. This stabilizing effect will significantly lower the energy barriers in Figure 4.

The presence of a ring-opened structure was further evaluated using H/D exchange. This technique allows the barrier for internal proton transfer or the proton affinity difference between the two deprotonated species (i.e., $DO^-$ and $C_3H_2N_3^-$) to be assessed. An endothermic gas phase H/D exchange process can be driven by the complexation energy ($\Delta H_{complexation}$~15–20 kcal $mol^{-1}$) within an ion-dipole complex. Based on the computational proton affinities at the B3LYP/6-311++G** level of theory for the isomeric forms of 1,3,5-triazinide [386.7 kcal $mol^{-1}$ for (1), 356.8 kcal $mol^{-1}$ for (2), and 356.1 kcal $mol^{-1}$ for (2′)] relative to the experimental proton affinity of hydroxide [390.3 kcal $mol^{-1}$] the only ion-dipole complex capable of undergoing H/D exchange is the ring-closed form (1) as shown in Scheme 1. Experimentally, the $C_3H_2N_3^-$ anion formed from both $HO^-$ and $CH_3O^-$ deprotonation showed two H/D exchanges with $D_2O$ (inset, Figure 2a) strongly suggesting that the ring-closed Structure (1) is the dominant species. The experimental and computational data indicate that the mechanistic reaction pathways most likely proceed through an intact 1,3,5-triazinide or triazine structure.

All of the carbanion [$C_4H_7^-$, $C_4H_3N_2^-$, $C_4H_3O^-$, $C_5H_4N^-$, $FC_6H_4^-$, $F_2C_6H_3^-$, $(CH_3)_2C_6H_3^-$, $(CH_3)C_4H_2O^-$] reactions with 1,3,5-triazine resulted almost exclusively in the formation of a stabilized ion-dipole complex. CID of these carbanion complexes did not display an addition-fragmentation pathway, only deprotonated forms of the anionic species. However, the ratio of CID fragment ions did not correlate with relative proton affinities as would be expected by kinetic method techniques. The method generally assumes that the peak intensities reflect the difference in Gibbs free energy between the transition state of a proton-bound complex and the two competing dissociation channels.

One would expect a decreasing ratio of carbanions to 1,3,5-triazinide as the proton affinity of the carbanion increases; nonetheless, in all cases, a majority of the 1,3,5-triazinide (>90%) retained the proton (see supporting information for relative abundances). This deviation from thermodynamic relationships indicates either a significant barrier to proton transfer or a non-proton bound form of ion-dipole complex (this aspect is discussed below).

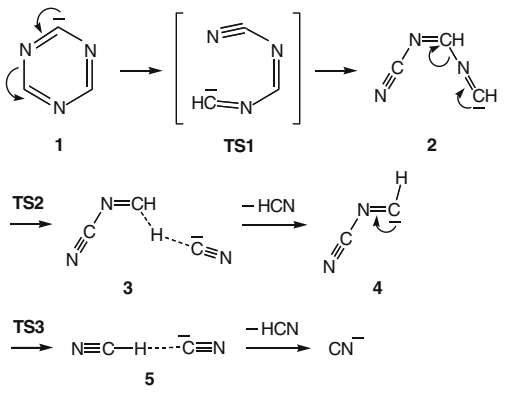


Scheme **2.** Dissociation scheme for the fragmentation of 1,3,5-triazinide

## *Reactivity of 1,3,5-Triazine*

The gas phase reactions formed a number of primary and secondary products; the latter tend to be anionic clusters with the neutral reactant. Table 1 lists the series of 1,3,5-triazine (M) reactions along with the corresponding proton affinity [54] of the reactant anion ($X^-$), the overall rate constant, reaction efficiency, and the initial product ion distribution. The primary product ions in Table 1 correspond to a proton transfer reaction, $(M–H)^-$, a stabilized anion-arene complex ($X^-$·M), a hydride transfer reaction $(M + H)^-$, and a fragmentation pathway (*m/z* 71, 44, 26) originating from an $S_NAr$ process. The carbanion reactions displayed only traces (<1%) of deprotonated 1,3,5-triazine $(M–H)^-$. The *m/z* 44 peak is only observed in reactions with

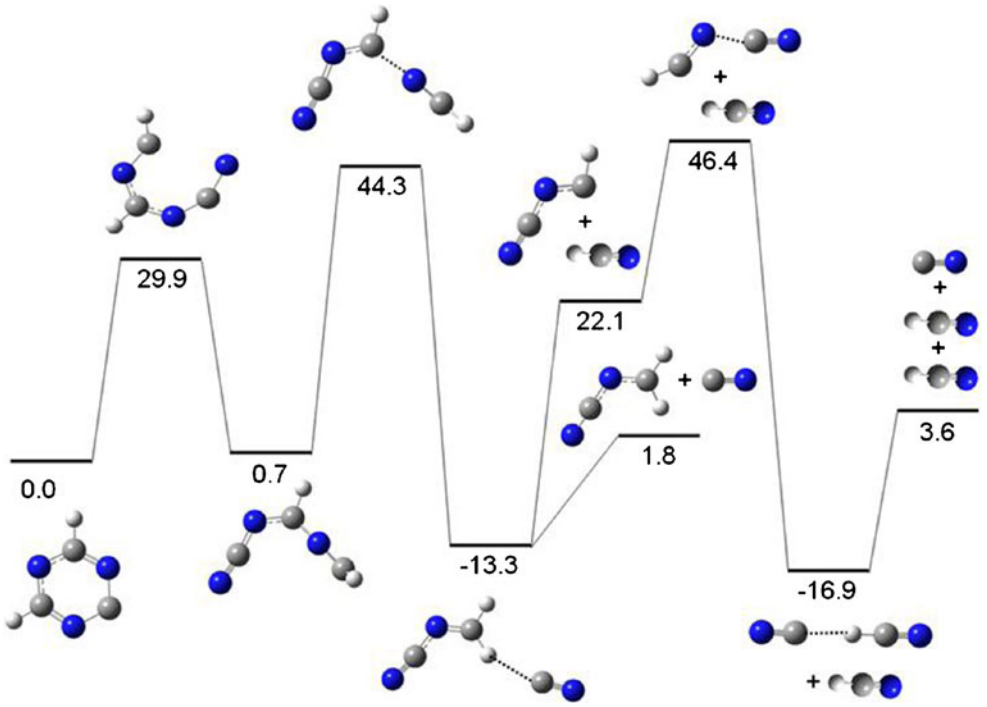


**Figure 4.** Energy diagram for the decomposition of 1,3,5-triazinide. Calculations performed at the B3LYP/6-311++G(d,p) level of theory (kcal $mol^{-1}$)

oxyanions. The additional peak observed at *m/z* 71 for the reaction with $HO^-$ corresponds to a loss of HCN from the reactant ion-dipole complex (*m/z* 98).

Our data show both the proton transfer and the addition $S_NAr$ pathways to be active. This is expected since the acidities of 1,3,5-triazine and the nucleophiles are similar as discussed in the introduction. Variations in product ion distribution can be interpreted as a competition between the exit channel for proton transfer and conversion within the ion-dipole complex. Normally this competition is between exit channels, however the elimination step of the $S_NAr$ mechanism for 1,3,5-triazine is thermodynamically inhibited since hydride is such a poor leaving group. We will simplify our discussion by treating the stabilized anion-arene complex, ($X^-$·M), as a single isomer composed of the anionic σ-adduct. Although a small amount of the proton-bound isomer exists, computations (see below) suggest that the Meisenheimer complex is significantly lower in energy

**Table 1.** 1,3,5-triazine (M) Reactions at 298 K with Proton Affinity (kcal $mol^{-1}$), Overall Rate Constant ($k_{expt}$)[a] in Units of $10^{-10}$ $cm^3$ $s^{-1}$, Reaction Efficiency ($Eff=k_{expt}/k_{col}$)[b], and Initial Product Ion Distribution

| Reaction | Proton affinity ($X^-$)[c] | Kinetic data | | Product ions (%) | | | | | |
|---|---|---|---|---|---|---|---|---|---|
| | | $k_{expt}$ | Eff | $(M-H)^-$ | $(X^-·M)$ | $(M+H)^-$ | (m/z 71) | (m/z 44) | (m/z 26) |
| $NH_2^- + C_3N_3H_3$ | 403.4±0.1 | 15.1±0.3 | 0.85 | 92 | 8 | | | | |
| $OH^- + C_3N_3H_3$ | 389.5±0.1[e] | 14.5±0.5 | 0.83 | 60 | 25 | | 2 | 10 | 3 |
| $CH_3O^- + C_3N_3H_3$ | 381.5±0.7[e] | 8.40±0.08[d] | 0.61 | 7 | 49 | 31 | | 12 | |
| $C_2H_5O^- + C_3N_3H_3$ | 378.3±0.8 | 7.20±0.01 | 0.60 | | 60 | 40 | | | |
| $C_5H_9O^- + C_3N_3H_3$ | 375.0±1.1[e] | — | — | | 75 | | | 25 | |
| carbanion[f] $+ C_3N_3H_3$ | 381.9-393.0 | — | — | 1 | 99 | | | | |
| $C_3N_3H_2^- + H_2O$[g] | 386.1±0.7 | — | — | | 100 | | | | |
| $C_3N_3H_2^- + CH_3OH$[g] | 386.1±0.7 | 10.7±0.1[d] | 0.53 | 100 | | | | | |

[a]Error bars represent one standard deviation of the mean of three or more measurements; absolute accuracy is ±20%.
[b]Efficiency is the ratio of the experimental rate constant to the collision rate constant calculated using parameterized trajectory collision theory [43].
[c]NIST Chemistry WebBook, NIST Standard Reference Database Number 69 [53], except where otherwise noted.
[d]Previous work [56].
[e]$HO^-$ [58], $CH_3O^-$ [58], $C_5H_9O^-$ this work.
[f]Carbanions [$C_4H_7^-$, $C_4H_3N_2^-$, $C_4H_3O^-$, $C_5H_4N^-$, $FC_6H_4^-$, $F_2C_6H_3^-$, $(CH_3)_2C_6H_3^-$, $(CH_3)C_4H_2O^-$].
[g]Fragmentation upon injection of 1,3,5-triazinide produced ~10% $CN^-$, however this ion did not participate in the primary reactions.

(consistent with the strong stabilizing effect of electron-withdrawing nitrogen) than the H-bonded complex and would dominate a Boltzmann distribution at equilibrium.

The product ion distributions for the gas phase anionic reactions with 1,3,5-triazine can be interpreted as a competition between a proton transfer pathway and the addition mechanism of the $S_NAr$ reaction. Most gas phase ion-molecule reaction mechanisms are represented by a double-well potential energy curve [55] where ion-dipole interactions form a potential minimum before significant changes in chemical bonding occurs in the central barrier. Often, there is more than one energetically accessible potential minimum within the reactant-ion dipole complex. As the nucleophile ($X^-$) approaches the arene, either a H-bonding or an electrostatic interaction develops along a minimum energy reaction pathway leading to two different reactant ion-dipole complexes, an aryl H-bonded complex and a Meisenheimer complex. Most proton transfer reactions have very low transition state barriers producing single-well reaction characteristics. Based on this single-well feature, the reactivity of proton transfer has direct correlations with the relative proton affinity of an anion. On the other hand, the $S_NAr$ (addition-elimination) reaction proceeds by nucleophilic attack on an electrophilic carbon to produce a resonance-stabilized Meisenheimer complex. (The hydride transfer reaction is an alternate pathway from the H-bonded complex driven by the exothermic formation of an aldehyde, see pathway below). A conversion barrier between the two pathways is highly likely based on previously reported calculations which suggest that large barriers may exist between binding motifs [56]. The presence of a conversion barrier is reasonable based on the large geometry changes and shifts in electron density between the σ-adduct and H-bonded complexes. Based on this overall picture, when an ion-dipole complex is formed there are three possible outcomes: dissociation back into reactants, an ensuing proton/hydride transfer (if the exit barrier is low enough), or stabilization through collisions with the carrier gas (if the lifetime of the complex is long enough).

As anticipated, there is a strong correlation between the degree of proton transfer and the relative gas phase proton affinity between 1,3,5-triazinide ($\Delta_{acid}H_{298}$=386.1±0.7 kcal mol$^{-1}$) [53] and the anions (non-carbon centered). The high proton affinity of $NH_2^-$ ($\Delta_{acid}H_{298}$=403.40±0.10 kcal mol$^{-1}$) [57] generates a highly exothermic pathway to the ammonia and triazinide products. The proton transfer rate constant for reaction of amide with 1,3,5-triazine is $k_{PT}=1.4\times10^{-9}$ cm$^3$ s$^{-1}$ ($k_{PT}=k_{expt}$ × branching fraction) with a reaction efficiency of 80%. With this large thermodynamic driving force of 17.3 kcal mol$^{-1}$ one would expect near collision rate reaction efficiency. The lower reaction efficiency observed and the presence of a stable complex suggest that conversion between the two reaction pathways is inhibited and reaction rates can be influenced by the type of anion-arene complexes that are energetically accessible.

The proton transfer rate constant for reaction of $HO^-$ ($\Delta_{acid}H_{298}$=389.5±0.1 kcal mol$^{-1}$) [58] with 1,3,5-triazine is $k_{PT}=8.7\times10^{-10}$ cm$^3$ s$^{-1}$ with a reaction efficiency of 50%. This reaction is exothermic by only 3.4 kcal mol$^{-1}$ and formation of the anionic σ-adduct becomes competitive; the product ion ratios are 60% proton transfer and 40% Meisenheimer complex (25% stable complex and 15% fragmentation). Proton transfer becomes endothermic by 4.6 kcal mol$^{-1}$ for $CH_3O^-$ ($\Delta_{acid}H_{298}$=381.5±0.7 kcal mol$^{-1}$) [58] and $k_{PT}=5.9\times10^{-11}$ cm$^3$ s$^{-1}$ with a reaction efficiency of 4%.

The reaction of cyclopentoxide does not result in proton transfer, however our forward and reverse rate measurements relative to isopropanol ($k_f=2.4\pm0.6\times10^{-11}$ cm$^3$ s$^{-1}$; $k_r=3.28\pm0.14\times10^{-10}$ cm$^3$ s$^{-1}$) give thermodynamic values of $\Delta_{acid}G_{298}$=366.9±1.1 kcal mol$^{-1}$ and $\Delta_{acid}H_{298}$=375.0±1.1 kcal mol$^{-1}$. These measurements indicate that cyclopentanol is considerably more acidic than reported by previous studies ($\Delta_{acid}H_{298}$=383.0±4.6 kcal mol$^{-1}$) [59]. Therefore, when the endothermicity is greater than 4.6 kcal mol$^{-1}$, proton transfer for anions with 1,3,5-triazine is below the detection limits of our instrument ($k_{PT} < 1\times10^{-12}$ cm$^3$ s$^{-1}$).

The dominance of the proton transfer channel when the reaction is highly exothermic is consistent with other gas phase work. For example, Briscese and Riveros [24, 26] observed exclusive proton transfer and complete inhibition of the $S_NAr$ reaction in their flourobenzene systems when proton transfer was about 9 kcal mol$^{-1}$ exothermic. It is therefore intriguing that the Meisenheimer complex was observable in our studies of $NH_2^-$ + 1,3,5-triazine where the acidity difference is 17 kcal mol$^{-1}$; this result suggests inhibition from conversion barriers and/or a more stable Meisenheimer complex. The enhanced stabilization is consistent with computations that have shown significant stabilization energies for anionic σ-complexes containing nitro groups relative to other electron-withdrawing groups [20, 60].

A hydride transfer channel becomes active for methoxide and is a major product channel for ethoxide. The hydride transfer rate constant ($k_{HT}$) for reaction of $CH_3O^-$ with 1,3,5-triazine is $k_{HT}=2.6\times10^{-10}$ cm$^3$ s$^{-1}$ ($k_{HT}=k_{expt}$ × branching fraction) with a reaction efficiency of 19%. The hydride transfer rate constant for reaction of $C_2H_5O^-$ with 1,3,5-triazine is $k_{HT}=2.9\times10^{-10}$ cm$^3$ s$^{-1}$ with a reaction efficiency of 24%.

Another insightful trend in the data shows that as the proton transfer channel is less available there is an increase in both a stabilized anion-arene complex ($X^-$·M) and fragmentation products. Based on the diagram of the reaction system (Figure 5), one may envision the increase in a stabilized complex due to an increase in "trapped" H-bonded complex. However, the increase in fragmentation products from an additive pathway (*m/z* 44, see CID section) indicates an increase in Meisenheimer complex. While the amide results indicate that conversion between binding motifs is inhibited, an increase in Meisenheimer complexes

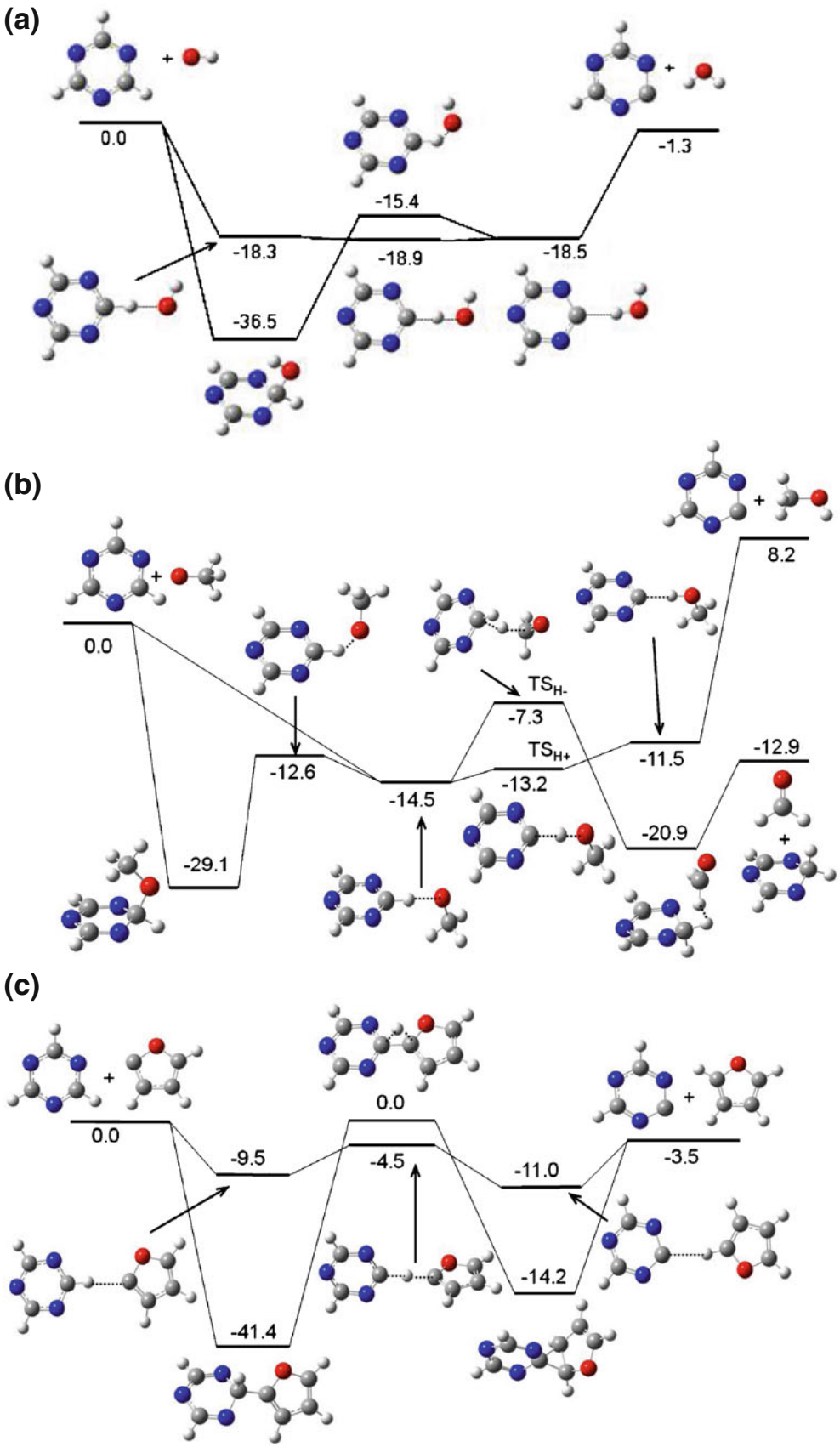


**Figure 5.** Reaction coordinate plots for the reaction of 1,3,5-triazine with (**a**) hydroxide, (**b**) methoxide, and (**c**) furanide. Calculations performed at the B3LYP/aug-cc-pVTZ level of theory. Energy values at 0 K are relative to separated reactants in units of kcal mol$^{-1}$

in less exothermic or more endothermic reactions suggests that although inhibited, conversion between anion-arene complexes is energetically accessible.

### *Potential Energy Surface of 1,3,5-Triazine Reactions*

To help characterize the mechanisms in the reactions of 1,3,5-triazine, DFT calculations were carried out using the Gaussian 09 suite of programs. Due to the wide variation in the ions and molecules studied, we were unable to find a level of theory that was capable of accurately reproducing enthalpies of deprotonation for all species. However, the B3LYP/aug-cc-pVTZ calculations for the cyclic compounds (1,3,5-triazine and furan) and the relative values for $H_2O$ versus $CH_3OH$ were within 1 kcal mol$^{-1}$ of the experimental gas phase acidity values; therefore differences between calculated energies should be fairly accurate. Reaction coordinate plots with optimized structures and associated energies at 0 K for the reaction of 1,3,5-triazine with (a) hydroxide, (b) methoxide, and (c) furanide are shown in Figure 5.

The reaction profile for $HO^-$ + $C_3H_3N_3$ (Figure 5a) clearly depicts potential energy minima for an aryl H-bonded complex and a relatively more stable Meisenheimer complex along different reaction pathways which lead to the same products, deprotonated triazine and water. Although not depicted, a hydrogen migration from the oxygen to the nitrogen in the Meisenheimer complex similar to those seen by Mukherjee and Ren [61], produces a stable keto-like ring opened structure (−40.2 kcal mol$^{-1}$). The barrier to this process lays 7.3 kcal mol$^{-1}$ below the total energy of reactants and may be the pathway that leads to the observed fragmentation products. The H-bonded complex proceeds through the typical "single-well" proton transfer pathway, while the anionic σ-adduct follows a gas-phase ion–molecule reaction double-minimum potential. The transition state for the proton transfer channel (−18.9 kcal mol$^{-1}$) and the central barrier (−15.4 kcal mol$^{-1}$) for the double-well are close in energy and well below the product energy (−1.3 kcal mol$^{-1}$). This suggests that both channels contribute to products and display single-well characteristics controlled primarily by the exothermicity of reaction.

Before collisional stablization, the ion–dipole complex should be able to freely convert between binding motifs given the potential energy surface for the hydroxide-triazine reaction (Figure 5a) and the conversion barrier should have no influence on the reaction. We would expect a similar conversion barrier for the amide-triazine reaction, however this does not explain the experimental data that suggest an inhibited reaction. A reasonable explanation accounting for the presence of a collisionally stabilized complex and inhibited efficiency originates from the large exothermicity of reaction. While hydroxide participates in a slightly exothermic proton transfer process, proton transfer with amide is highly exothermic. As a result of the stability of the products, proton transfer through the anionic σ-adduct for amide has double-well characteristics with the conversion barrier inhibiting and controlling the reaction pathway. Computations for $NH_2^-$ + 1,3,5-triazine support this view (see supporting information) with the anionic σ-adduct (−44.0 kcal mol$^{-1}$) and H-bonded product ion-dipole complex (−23.2 kcal mol$^{-1}$) lying below the conversion barrier (−15.7 kcal mol$^{-1}$).

The reaction profile for $CH_3O^-$ + $C_3H_3N_3$ (Figure 5b) also indicates the presence of an aryl H-bonded complex and a relatively more stable Meisenheimer complex. The H-bonded complex and anionic σ-adduct follow single-well characteristics to proton transfer products and a double-well potential leading to hydride transfer products. The proton transfer process is endothermic and is expected to be extremely slow. The alternate hydride transfer pathway is exothermic by 12.9 kcal mol$^{-1}$ and should be the dominant channel kinetically controlled by the slightly higher central barrier (−7.3 kcal mol$^{-1}$). This relationship is observed in the product ion ratios of 7% proton transfer and 31% hydride transfer.

The presence of a hydride transfer pathway is intriguing, since often competing processes can interfere with detection of this mechanism. Hydride transfer involves motion of a proton with an electron pair between electron deficient sites. The hydride affinities for closed shell neutrals range from 6 to 106 kcal mol$^{-1}$ [62]. Our computations suggest that the hydride affinity of 1,3,5-triazine is 52 kcal mol$^{-1}$ (similar to acrylonitile, $C_3H_3N$, at 56 kcal mol$^{-1}$ [62]) indicating a moderately strong bonding interaction between the $1s^2$ electrons of the hydride and the π* orbitals. Gronert and Keefe discuss this "in phase" interaction within a three-nuclei (C•••H•••C) transition state framework in terms of maxim overlap to account for non-linear geometries [41]. Our calculated bond angle (157°) and the overlap of the HOMO for the methoxide reaction depict this type of constructive interaction. Weak hydrogen bonding between the oxygen of the anion and the hydrogen attached to the carbon at the site of attack may facilitate this orientation of the transition state as well as lower the overall energy. In addition to high hydrogen binding energies, hydride acceptors tend to have high electron binding energies. Computations suggest that the electron-withdrawing character of –CN and $–NO_2$ groups produce very stable hydride adducts corresponding to positive electron affinities (2.4 kcal mol$^{-1}$ and 27.7 kcal mol$^{-1}$, respectively) [63]. The nitrogen atoms in the 1,3,5-triazine ring should have a similar effect on the electron affinity by shifting electron density away from the nearby reaction center reducing the Coulombic repulsive forces and increasing the effective nuclear charge. Furthermore, negative charge delocalization at the nitrogen positions and resonance within the ring help stabilize the additional electron density in the anionic product and transition state structures.

The reaction profile for $C_4H_3O^-$ + $C_3H_3N_3$ (Figure 5c) provides insight into the lack of proton transfer for the

carbanion reactions. The potential energy profile for the proton transfer reaction displays double-well characteristics. Analogous to the hydride transfer process, the proton transfer can also be viewed as a three-nuclei array in which the HOMO is antibonding resulting in an electrostatically controlled reaction (shuttling of the proton between two atoms with electron pairs) [41]. The degree of stability in this "ionic" transition state $[Ar^{-}\cdots H^{+}\cdots X^{-}]^{\ddagger}$ correlates with the electronegativity of the attacking atom of the nucleophile [64]. Due to high electronegativity, amide and oxyanions concentrate electron density to generate strong electrostatic attractions and low transition state barriers. Carbanions are less capable of shifting electron density, which results in weak electrostatic forces in the transition states and barriers to proton transfer. Furthermore, while electron-withdrawing nitrogen and delocalization in 1,3,5-triazine weakens the C-H bond, this also reduces the stabilizing electrostatic/H-bonding interactions (very small $\delta^{-}$ on carbon site in $Ar^{-}$) in the transition state. These factors combine to generate activation barriers to proton transfer between carbon centers. Thus, even with a large thermodynamic driving force, the furanide ($\Delta_{acid}H_{298}$=391.10±0.40 kcal mol$^{-1}$) [65] reaction has a transition state barrier of 5 kcal mol$^{-1}$ above the H-bonded complex inhibiting and slowing the reaction. Essentially the ion-dipole complex is trapped in either a H-bonded complex well or an anionic σ-adduct. The energy diagram indicates the anionic σ-adduct is over 30 kcal mol$^{-1}$ more stable than the H-bonded complex, and therefore is statistically favored. This trapping of the ion-dipole complex prohibits thermodynamically controlled conversion between proton bound forms resulting in the lack of deprotonated 1,3,5-triazine in our CID studies.

One final aspect revealed in our computations (see supporting information for specific bond lengths and angles of the Meisenheimer complexes) is the slight distortion of the aromatic ring ($sp^3$ bond angle character range of the Nu–C–H bonds is 99–108°, and dihedral angle range of the $C_{Nu}$–plane of ring is 7–10°, where $C_{Nu}$ is the site of nucleophilic addition) and the short adduct bond lengths (<1.5 Å, covalent). Therefore, all of the Meisenheimer complexes formed are in the strong σ-adduct category. This result is expected due to the strong bond energies associated with C–N, C–C, and C–O bonds. In addition, the exceptionally high stability of these adducts is generated by the symmetric nature of the ring where most of the electron density is localized at the nitrogen positions, thereby delocalizing the charge over the entire ring.

## Conclusion

Our investigation of the reactions of 1,3,5-triazine has provided a more detailed understanding of the influence of anion-arene interactions on mechanisms and product distributions in the gas phase. Analysis of reactivity trends, collision induced fragmentation processes and H/D exchange experiments revealed intriguing structure–reactivity relationships generated by the electron-withdrawing character of the heteroaromatic nitrogen. The major conclusions drawn from this work include the following.

(1) A multi-step and/or single-step ring-opening collision-induced fragmentation appears to exist for 1,3,5-triazinide, similar to the photodissociation pathways reported for neutral 1,3,5-triazine.
(2) The electron-withdrawing nitrogen atoms in the 1,3,5-triazine ring significantly reduce Coulombic repulsive forces to generate extremely electrophilic carbon centers. The presence of a major hydride transfer process indicates the strength of this effect.
(3) The symmetric nature of the nitrogen atoms in the ring allows stabilization of the negative charge density in the anionic products through delocalization over the entire ring. This effect is manifested in the high stability of the strong covalent σ-adducts.
(4) The $S_NAr$ addition pathway in 1,3,5-triazine is competitive over a wider range of relative gas phase acidity differences than previously reported for other aromatic systems.
(5) Our data suggest that the type of interactions initially formed in the loose anion–arene complexes and the transition state barriers between binding motifs can significantly influence competition between different channels which may be operative in gas-phase reactions.

## Acknowledgments

The authors gratefully acknowledge support of this work by the National Science Foundation (CHE 1012321) and the AFOSR (FA9550-09-1-0046). J.M.G. respectfully acknowledges the sponsorship and support of the Air Force Institute of Technology. The computational work was supported by an allocation through the TeraGrid Advanced Support Program. The authors appreciate the insightful discussions with Professor Charles H. DePuy.

## References

1. Agrawal, J.P.: Recent trends in high-energy materials. *Progr. Energy Combust. Sci.* **24**, 1–30 (1998)
2. Alves, W.A.: Formamide complexes with selected azabenzenes: A discussion on their thermodynamic properties from Raman analyses. *Vib. Spectrosc.* 53, 285–288 (2010)
3. Ali, T.E.S.: Synthesis of some novel pyrazolo[3,4-b]pyridine and pyrazolo[3,4-d]pyrimidine derivatives bearing 5,6-diphenyl-1,2,4-triazine moiety as potential antimicrobial agents. *Eur. J. Med. Chem.* **44**, 4385–4392 (2009)
4. Pelizzetti, E., Maurino, V., Minero, C., Carlin, V., Pramauro, E., Zerbinati, O., Tosato, M.L.: Photocatalytic degradation of atrazine and other s-triazine herbicides. *Environ. Sci. Technol.* **24**, 1559–1565 (1990)
5. Eisa, H.M., Tantawy, A.S., Elkerdawy, M.M.: Synthesis of certain 2-aminoadamantane derviatives as potential antimicrobial agents. *Pharmazie* **46**, 182–184 (1991)
6. Klenke, B., Stewart, M., Barrett, M.P., Brun, R., Gilbert, I.H.: Synthesis and biological evaluation of s-triazine substituted polyamines as potential new anti-trypanosomal drugs. *J. Med. Chem.* **44**, 3440–3452 (2001)

7. Valet, A.: Outdoor applications of UV curable clearcoats - a real alternative to thermally cured clearcoats. *Prog. Org. Coat.* **35**, 223–233 (1999)
8. Rogers, J., Moyer, B., Kalscheur, G., Emig, N.: Advanced light stabilizers for the next century's needs. *JCT Coatingstech* **4**, 82–86 (2007)
9. Turker, L., Atalar, T., Gumus, S., Camur, Y.: A DFT study on nitrotriazines. *J. Hazard. Mater.* **167**, 440–448 (2009)
10. Berryman, O.B., Johnson, D.W.: Experimental evidence for interactions between anions and electron-deficient aromatic rings. *Chem. Commun. (Cambridge, UK)* 3143–3153 (2009)
11. Wheeler, S.E., Houk, K.N.: Are anion/pi interactions actually a case of simple charge–dipole Interaction? *J. Phys. Chem. A* 114, 8658–8664 (2010)
12. Ciesielski, A., Krygowski, T.M., Cyranski, M.K., Dobrowolski, M.A., Balaban, A.T.: Are thermodynamic and kinetic stabilities correlated? A Topological Index of Reactivity toward Electrophiles Used as a Criterion of Aromaticity of Polycyclic Benzenoid Hydrocarbons. *J. Chem. Inf. Model* **49**, 369–376 (2009)
13. Katritzky, A.R., Barczynski, P., Musumarra, G., Pisano, D., Szafran, M.: Aromaticity as a quantitative concept. 1. A statistical demonstration of the orthogonality of classical and magnetic aromaticity in 5-membered and 6-membered heterocycles. *J. Am. Chem. Soc.* **111**, 7–15 (1989)
14. Schlosser, M., Ruzziconi, R.: Nucleophilic Substitutions of Nitroarenes and Pyridines: New Insight and New Applications. *Synthesis-Stuttgart* **13**, 2111–2123 (2010)
15. Mąkosza, M.: Electrophilic and nucleophilic aromatic substitution: Analogous and complementary processes. *Russ. Chem. Bull.* **45**, 491–504 (1996)
16. Dillow, G.W., Kebarle, P.: Fluoride Affinities of perfluorobenzenes $C_6F_5X$ - Meisenheimer complexes in the gas-phase and solution. *J. Am. Chem. Soc.* **110**, 4877–4882 (1988)
17. Zheng, Y.J., Ornstein, R.L.: Mechanism of nucleophilic aromatic substitution of 1-chloro-2,4-dinitrobenzene by glutathione in the gas phase and in solution. Implications for the mode of action of glutathione S-transferases. *J. Am. Chem. Soc.* **119**, 648–655 (1997)
18. Giroldo, T., Xavier, L.A., Riveros, J.M.: An unusually fast nucleophilic aromatic displacement reaction: The gas-phase reaction of fluoride ions with nitrobenzene. *Angew. Chem.* **43**, 3588–3590 (2004)
19. Chiavarino, B., Crestoni, M.E., Fornarini, S., Lanucara, F., Lemaire, J., Maitre, P.: Meisenheimer complexes positively characterized as stable intermediates in the gas phase. *Angew. Chem.* **46**, 1995–1998 (2007)
20. Fernández, I., Frenking, G., Uggerud, E.: Rate-Determining Factors in Nucleophilic Aromatic Substitution Reactions. *J. Org. Chem.* **75**, 2971–2980 (2010)
21. Hay, B.P., Bryantsev, V.S.: Anion-arene adducts: C–H hydrogen bonding, anion–pi interaction, and carbon bonding motifs. *Chem. Commun. (Cambridge, U. K.)* 2417–2428 (2008)
22. Hiraoka, K., Mizuse, S., Yamabe, S.: High-Symmetrical Structure of the Gas-Phase Cluster Ions $X^-\ldots C_6F_6$ (X=Cl, Br, and I). *J. Phys. Chem.* **91**, 5294–5297 (1987)
23. Chiavarino, B., Crestoni, M.E., Fornarini, S., Lanucara, F., Lemaire, J., Maitre, P., Scuderi, D.: Molecular Complexes of Simple Anions with Electron-Deficient Arenes: Spectroscopic Evidence for Two Types of Structural Motifs for Anion-Arene Interactions. *Chem. Eur. J.* **15**, 8185–8195 (2009)
24. Briscese, S.M.J., Riveros, J.M.: Gas phase nucleophilic reactions of aromatic systems. *J. Am. Chem. Soc.* **97**, 230–231 (1975)
25. Schneider, H., Vogelhuber, K.M., Schinle, F., Weber, J.M.: Aromatic molecules in anion recognition: Electrostatics versus H-bonding. *J. Am. Chem. Soc.* **129**, 13022–13026 (2007)
26. Chen, H., Chen, H.W., Cooks, R.G.: Meisenheimer complexes bonded at carbon and at oxygen. *J. Am. Soc. Mass Spectrom.* **15**, 998–1004 (2004)
27. Paul, G.J.C., Kebarle, P.: Stabilities of complexes of $Br^-$ with substituted benzenes (SB) based on determinations of the gas phase equilibria $Br^- + SB=(BrSB)^-$. *J. Am. Chem. Soc.* **113**, 1148–1154 (1991)
28. Danikiewicz, W., Bienkowski, T., Kozlowska, D., Zimnicka, M.: Aromatic nucleophilic substitution ($S_NAr$) reactions of 1,2- and 1,4-halonitrobenzenes and 1,4-dinitrobenzene with carbanions in the gas phase. *J. Am. Soc. Mass Spectrom.* **18**, 1351–1363 (2007)
29. Ingemann, S., Nibbering, N.M.M., Sullivan, S.A., DePuy, C.H.: Nucleophilic aromatic-substitution in the gas phase—the importance of $F^-$ ion molecule complexes formed in gas phase reactions between nucleophiles and some alkyl pentafluoro phenyl ethers. *J. Am. Chem. Soc.* **104**, 6520–6527 (1982)
30. Khan, H., Harris, R.J., Barna, T., Craig, D.H., Bruce, N.C., Munro, A. W., Moody, P.C.E., Scrutton, N.S.: Kinetic and structural basis of reactivity of pentaerythritol tetranitrate reductase with NADPH, 2-cyclohexenone, nitroesters, and nitroaromatic explosives. *J. Biol. Chem.* **277**, 21906–21912 (2002)
31. Behrend, C., Heesche-Wagner, K.: Formation of hydride-Meisenheimer complexes of picric acid (2,4,6-trinitrophenol) and 2,4-dinitrophenol during mineralization of picric acid by Nocardioides sp. strain CB 22–2. *Appl. Environ. Microbiol.* **65**, 1372–1377 (1999)
32. Vorbeck, C., Lenke, H., Fischer, P., Knackmuss, H.J.: Idenfitication of a hydride-Meisenheimer complex as a metabolite of 2,4,6-trinitrotoluene by mycobacterium strain. *J. Bacteriol.* **176**, 932–934 (1994)
33. Ziganshin, A.M., Gerlach, R., Borch, T., Naumov, A.V., Naumova, R. P.: Production of eight different hydride complexes and nitrite release from 2,4,6-Trinitrotoluene by Yarrowia lipolytica. *Appl. Environ. Microbiol.* **73**, 7898–7905 (2007)
34. Rieger, P.G., Sinnwell, V., Preuss, A., Francke, W., Knackmuss, H.J.: Hydride-Meisenheimer complex formation and protonation as key reactions of 2,4,6-trinitrophenol biodegradation by Rhodococcus erythropolis. *J. Bacteriol.* **181**, 1189–1195 (1999)
35. Yinon, J., Johnson, J.V., Bernier, U.R., Yost, R.A., Mayfield, H.T., Mahone, W.C., Vorbeck, C.: Reactions in the mass-spectrometry of a hydride Meisenheimer complex of 2,4,6-trinitrotoluene. *J. Mass Spectrom.* **30**, 715–722 (1995)
36. Artau, A., Ho, Y., Kenttamaa, H., Squires, R.R.: Diastereoselectivity in gas-phase hydride reduction reactions of ketones. *J. Am. Chem. Soc.* **121**, 7130–7137 (1999)
37. DePuy, C.H., Bierbaum, V.M., Schmitt, R.J., Shapiro, R.H.: Gas phase oxidation and reduction reactions with $C_6H_7^-$, $HNO^-$, and $HO_2^-$. *J. Am. Chem. Soc.* **100**, 2920–2921 (1978)
38. Ingemann, S., Kleingeld, J.C., Nibbering, N.M.M.: Reduction reactions with methoxide ion in the gas phase. *J. Chem. Soc., Chem. Commun.* 1009–1011 (1982)
39. Bernasconi, C.F., Stronach, M.W., DePuy, C.H., Gronert, S.: Gas phase acidities of acrolein and methyl acrylate. *J. Phys. Org. Chem.* **3**, 346–348 (1990)
40. Bernasconi, C.F., Stronach, M.W., DePuy, C.H., Gronert, S.: Reactions of anions with activated olefins in the gas phase: A flowing afterglow selected ion flow tube study. *J. Am. Chem. Soc.* **112**, 9044–9052 (1990)
41. Gronert, S., Keeffe, J.R.: Identity hydride-lon transfer from C–H donors to C acceptor sites. Enthalpies of hydride addition and enthalpies of activation. Comparison with C…H…C proton transfer. An ab initio study. *J. Am. Chem. Soc.* **127**, 2324–2333 (2005)
42. Van Doren, J.M., Barlow, S.E., DePuy, C.H., Bierbaum, V.M.: The tandem flowing afterglow-SIFT-drift. *Int. J. Mass Spectrom. Ion Processes* **81**, 85–100 (1987)
43. Su, T., Chesnavich, W.J.: Parametrization of the Ion–Polar Molecule Collision Rate-Constant by Trajectory Calculations. *J. Chem. Phys.* **76**, 5183–5185 (1982)
44. Kato, S., Lineberger, W.C., Bierbaum, V.M.: Collision-induced dissociation of fluoropyridinide anions. *Int. J. Mass Spectrom.* **266**, 166–179 (2007)
45. Blanksby, S.J., Kato, S., Bierbaum, V.M., Ellison, G.B.: Fragmentations of deprotonated alkyl hydroperoxides ($ROO^-$) upon collisional activation: A combined experimental and computational study. *Aust. J. Chem.* **56**, 459–472 (2003)
46. Custer, T.G., Kato, S., Fall, R., Bierbaum, V.M.: Negative-ion CIMS: Analysis of volatile leaf wound compounds including HCN. *Int. J. Mass Spectrom.* **223**, 427–446 (2003)
47. Kato, S., DePuy, C.H., Gronert, S., Bierbaum, V.M.: Gas phase hydrogen/deuterium exchange reactions of fluorophenyl anions. *J. Am. Soc. Mass Spectrom.* **10**, 840–847 (1999)
48. DePuy, C.H., Kato, S.: H/D Exchange Reactions. In: Armentrout, P.B. (ed.) Encyclopedia of Mass Spectrometry: Theory and Ion Chemistry, pp. 670–674. Elsevier, Amsterdam (2003)
49. Gaussian 03 (Revision-B.05), Frisch, M. J.; Trucks, G. W.; Schlegel, H. B.; Scuseria, G. E.; Robb, M. A.; Cheeseman, J. R.; Montgomery, J. J. A.; Vreven, T.; Kudin, K. N.; Burant, J. C.; Millam, J. M.; Iyengar, S. S.; Tomasi, J.; Barone, V.; Mennucci, B.; Cossi, M.; Scalmani, G.; Rega, N.; Petersson, G. A.; Nakatsuji, H.; Hada, M.; Ehara, M.; Toyota, K.; Fukuda, R.; Hasegawa, J.; Ishida, M.; Nakajima, T.; Honda, Y.; Kitao, O.; Nakai, H.; Klene, M.; Li, X.; Knox, J. E.; Hratchian, H. P.; Cross, J. B.;

Bakken, V.; Adamo, C.; Jaramillo, J.; Gomperts, R.; Stratmann, R. E.; Yazyev, O.; Austin, A. J.; Cammi, R.; Pomelli, C.; Ochterski, J. W. A., P. Y.; Morokuma, K.; Voth, G. A.; Salvador, P.; Dannenberg, J. J.; Zakrzewski, V. G.; Dapprich, S.; Daniels, A. D.; Strain, M. C.; Farkas, O.; Malick, D. K.; Rabuck, A. D.; Raghavachari, K.; Foresman, J. B.; Ortiz, J. V.; Cui, Q.; Baboul, A. G.; Clifford, S.; Cioslowski, J.; Stefanov, B. B.; Liu, G.; Liashenko, A.; Piskorz, P.; Komaromi, I.; Martin, R. L.; Fox, D. J.; Keith, T.; Al-Laham, M. A.; Peng, C. Y.; Nanayakkara, A.; Challacombe, M.; Gill, P. M. W.; Johnson, B.; Chen, W.; Wong, M. W.; Gonzalez, C.; Pople, J. A. Gaussian, Inc.: Pittsburgh, PA, 2004

50. Ichino, T., Gianola, A.J., Kato, S., Bierbaum, V.M., Lineberger, W.C.: Structure of the vinyldiazomethyl anion and energetic comparison to the cyclic isomers. *J. Phys. Chem. A* **111**, 8374–8383 (2007)
51. Wiberg, K.B., Nakaji, D., Breneman, C.M.: Azines—a theoretical study of pi-electron delocalization. *J. Am. Chem. Soc.* **111**, 4178–4190 (1989)
52. Dyakov, Y.A., Mebel, A.M., Lin, S.H., Lee, Y.T., Ni, C.K.: Photodissociation of 1,3,5-triazine: An ab initio and RRKM study. *J. Phys. Chem. A* **111**, 9591–9599 (2007)
53. Wren, S.W., Vogelhuber, K.M., Garver, J.M., Kato, S., Sheps, L., Bierbaum, V.M., Lineberger, W.C.: manuscript in preparation.
54. Bartmess, J.E.: "Negative Ion Energetics Data" in NIST Chemistry WebBook, NIST Standard Reference Database Number 69, Linstrom, P.J and Mallard, W.G., Eds. National Institute of Standards and Technology: Gaithersburg, MD, 20899, http://webbook.nist.gov, (retrieved December 1, 2010).
55. Olmstead, W.N., Brauman, J.I.: Gas-phase nucleophilic displacement-reactions. *J. Am. Chem. Soc.* **99**, 4219–4228 (1977)
56. Dotterer, S.K., Harris, R.L.: MNDO study of nucleophilic aromatic-substitution. *J. Org. Chem.* **53**, 777–779 (1988)
57. Wickhamjones, C.T., Ervin, K.M., Ellison, G.B., Lineberger, W.C.: $NH_2$ Electron-Affinity. *J. Chem. Phys.* **91**, 2762–2763 (1989)
58. Ervin, K.M., DeTuro, V.F.: Anchoring the gas-phase acidity scale. *J. Phys. Chem. A* **106**, 9947–9956 (2002)
59. Alconcel, L.S., Continetti, R.E.: Dissociation dynamics and stability of cyclopentoxy and cyclopentoxide. *Chem. Phys. Lett.* **366**, 642–649 (2002)
60. Glukhovtsev, M.N., Bach, R.D., Laiter, S.: Single-step and multistep mechanisms of aromatic nucleophilic substitution of halobenzenes and halonitrobenzenes with halide anions: Ab initio computational study. *J. Org. Chem.* **62**, 4036–4046 (1997)
61. Mukherjee, S., Ren, J.H.: Gas-Phase Acid-Base Properties of Melamine and Cyanuric Acid. *J. Am. Soc. Mass Spectrom.* **21**, 1720–1729 (2010)
62. Goebbert, D.J., Wenthold, P.G.: Gas-phase hydride affinities of neutral molecules. *Int. J. Mass Spectrom.* **257**, 1–11 (2006)
63. Vianello, R., Peran, N., Maksic, Z.B.: Hydride affinities of substituted alkenes: Their prediction by density functional calculations and rationalization by triadic formula. *Eur. J. Org. Chem.* 526–539 (2007)
64. Keeffe, J.R., Gronert, S., Colvin, M.E., Tran, N.L.: Identity proton-transfer reactions from C–H, N–H, and O–H acids. An ab initio, DFT, and CPCM-B3LYP aqueous solvent model study. *J. Am. Chem. Soc.* **125**, 11730–11745 (2003)
65. Clifford, E.P., Wenthold, P.G., Lineberger, W.C., Ellison, G.B., Wang, C.X., Grabowski, J.J., Vila, F., Jordan, K.D.: Properties of tetramethyleneethane (TME) as revealed by ion chemistry and ion photoelectron spectroscopy. *J. Chem. Soc., Perkin Trans.* **2**, 1015–1022 (1998)